Improving Short-Term Numerical Weather Prediction in the California Coastal Zone by Dynamic Initialization of the Marine Boundary Layer

S. MARK LEIDNER,* DAVID R. STAUFFER, AND NELSON L. SEAMAN

The Pennsylvania State University, University Park, Pennsylvania

(Manuscript received 1 December 1999, in final form 30 May 2000)

ABSTRACT

Few data are available over the world's oceans to characterize the initial atmospheric state in numerical models. Objective analysis in these regions is largely based on forecast fields obtained from a global model and used as the background (''first guess''). Unfortunately, global models often do not resolve the marine boundary layer (MBL) structure, which is important for simulating stratus clouds, coastal zone circulations, and electromagnetic wave propagation. Furthermore, initialization of the MBL in the coastal zone and data-sparse oceanic regions poses a challenging mesoscale modeling problem. The goal of this study, therefore, is to improve warm-season short-term mesoscale numerical prediction of California coastal zone meteorology by improving the model initial conditions in the coastal zone and offshore data-void regions. Initialization strategies tested include standard static and dynamic techniques and a new marine boundary layer initialization scheme that uses a dynamic initialization based on the remarkably consistent summertime marine-layer climatology of the eastern Pacific Ocean.

The model used in this study is the Pennsylvania State University–National Center for Atmospheric Research fifth-generation Mesoscale Model (MM5). Experiments were performed for a typical summertime case (3–4 Aug 1990) to determine an initialization strategy suitable for coastal zone forecasting over the northeast Pacific. The meteorology in this case was dominated by quasi-stationary synoptic-scale high pressure over the ocean. Results from the model experiments were verified using 6-hourly coastal rawinsonde observations and visible range satellite cloud imagery.

More accurate initial conditions were obtained by using dynamic initialization compared to static initialization. The most accurate initialization and short-range model forecasts were produced by assimilating a combination of observed data over land and climatological information offshore during the 12-h preforecast period. Through the 24-h forecast period, errors in the coastal zone PBL depth and marine inversion strength were reduced by 65% and 41%, respectively, compared to the static-initialization control experiments. Without proper initialization of the offshore MBL, coastal zone forecasts degraded with time due to the long timescale of physical processes responsible for generating the MBL structure over cold, low-latitude oceans. Therefore, improvement of the model initial conditions in the California coastal zone by assimilation of climatological information offshore in combination with observed conditions near the coast proved to be an effective strategy for increasing short-range forecast accuracy.

1. Introduction

The cold waters of the northeast Pacific Ocean and the atmospheric marine boundary layer (MBL) off the west coast of the United States greatly influence the meteorology of the coastal zone. The coastal zone is defined here as the region 100 km from the coastline either inland or offshore (Rotunno et al. 1992). The sea breeze, the horizontal and vertical structure of boundary layer clouds and fog, and the coastal low-level jet structure (e.g., Chao 1985; Zemba and Friehe 1987; Gerber et al. 1989; Burk and Thompson 1996) are common examples of coastal zone meteorological phenomena influenced by the MBL. In addition, coastal zone meteorology directly impacts commerce and public safety via ship routing decisions, pollutant transport, ducting of radar and radio waves, and other meteorological disturbances such as the coastally trapped wind reversal (Dorman 1985; Bond et al. 1996; Mass and Bond 1996; Thompson et al. 1997b), the Catalina eddy (Mass and Albright 1987; Thompson et al. 1997a), and other observed phenomena (Winant et al. 1988; Dorman 1985). The west coast of the United States is especially affected by the MBL since a dominant flow regime is onshore.

Accurate forecasts in the California coastal zone depend on our knowledge of boundary layer conditions

* Current affiliation: Atmospheric and Environmental Research, Inc., Cambridge, Massachusetts.

Corresponding author address: S. Mark Leidner, Atmospheric and Environmental Research, Inc., 840 Memorial Drive, Cambridge, MA 02139.
E-mail: leidner@aer.com

upstream over the Pacific Ocean, but this offshore information is quite scarce. In situ observations including rawinsondes and buoy data are typically very limited and too sparse to adequately define the state of the MBL. Rawinsonde observations at the coast may be used in some situations to infer conditions offshore, but variable coastal wind directions and sloping marine layers limit their application over large distances. Satellite sounding data are improving, but are still not able to resolve the detailed vertical structure of the shallow MBL.

Numerical models are often used as another source of information offshore, but the quality of analyses from data assimilation systems in data-sparse regions is only as good as the background or first guess (i.e., model forecast) fields. For example, Ballard et al. (1991) investigated forecasting sea fog off the coast of Scotland using the United Kingdom Met. Office mesoscale model. They found that initial conditions with a background derived from the European Centre for Medium-Range Weather Forecasts (ECMWF) global model did not simulate the distribution of cloud water with sufficient accuracy for effective mesoscale model initialization. In another study (Bretherton et al. 1995), as part of the Atlantic Stratocumulus Transition Experiment field program, special MBL soundings were directly assimilated into the ECMWF global model's initial conditions. They showed that the overall MBL structure in the initial conditions was preserved in 5-day forecasts with some skill, but that cloud predictions made with several special cloud parameterizations showed little accuracy.

With these shortcomings in mind, the present study addresses the problem of mesoscale model initialization offshore where few data are routinely available. It is hypothesized that a combination of climatological and observed data can significantly improve the initial conditions and forecasts of the MBL in the coastal zone during the warm season when synoptic conditions over the northeast Pacific Ocean have generally low variance. The ultimate goal of this research is to improve short-range coastal zone forecasting. Toward that end, a case study representative of typical summertime conditions will be used in this preliminary evaluation designed to identify techniques suitable for subsuquent confirmation over many cases.

2. Description of the mesoscale modeling system

The Pennsylvania State University–National Center for Atmospheric Research (PSU–NCAR) fifth-generation Mesoscale Model (MM5) is used in this study. The MM5 is a nonhydrostatic, multinested, primitive equation mesoscale meteorological model described by Grell et al. (1994) and Dudhia (1993). In this application, nested grids are used with horizontal resolutions of 36 km and 12 km with 55 × 55 and 91 × 67 grid points, respectively (Fig. 1). Both grids have 30 nonuniformly spaced, terrain-following sigma (nondimensionalized pressure) layers in the vertical with 12 layers below 850 hPa and the model top at 100 hPa. The 36-km grid is approximately 2000 km × 2000 km centered on California, while the nested 12-km grid includes nearly the entire California coastline. Some of the important physiographic features of the region are the Serria Nevada on the eastern side of California and the Coast Range Mountains to the west, which flank the Sacramento Valley to the north of San Francisco Bay and the San Joaquin Valley to the south of the bay.

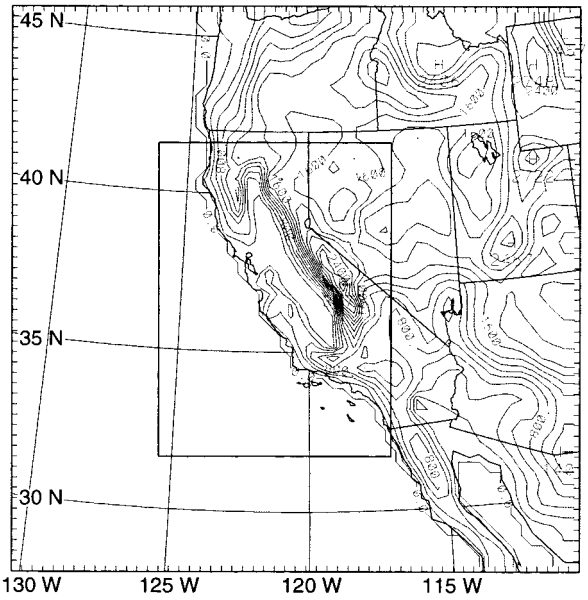

FIG. 1. Mesoscale model domains and terrain. Contour interval is 200 m.

Model physics

Several physical parameterizations were found to be essential for simulating the meteorology of the California coastal zone. A multilayer Blackadar planetary boundary layer (PBL) parameterization is used to represent turbulent processes (Zhang and Anthes 1982). Surface fluxes of heat, moisture, and momentum are computed from similarity theory. Surface temperature over land is predicted using a force–restore method based on the surface energy budget equation, while over the ocean, the sea surface temperature is specified from observations and held constant in time. Accurate simulation of the marine stratus is very important for obtaining realistic inversion-layer strength due to the effects of cloud-top cooling (e.g., Duynkerke and Driedonks 1987). Explicit moisture equations are used to predict grid-scale cloud and rainwater mixing ratios as well as water vapor (Dudhia 1989).

The atmospheric radiation module within MM5 includes longwave and shortwave schemes that interact with the atmosphere, cloud and precipitation fields, and with the surface (Dudhia 1989). Atmospheric longwave radiation is parameterized by a two-stream broadband

scheme. Shortwave radiation is parameterized to include clear-air scattering and absorption (Lacis and Hansen 1974), and cloud albedo and absorption (Stephens 1978).

Examination of the temperature tendency budget in MM5 produced by the Dudhia radiation scheme revealed that shortwave heating rates at cloud top for marine stratus were as much as twice the absolute value of the longwave cooling at solar noon. This resulted in net heating and had the effect of evaporating all MBL cloud water in MM5 within 1 h of solar noon, which is inconsistent with the persistent stratus cloud deck often observed off the West Coast. Numerous observational and modeling studies (Oliver et al. 1978; Stephens 1978; Duynkerke and Hignett 1993) of low-level stratus clouds have shown that even at solar noon, when shortwave heating is most intense, shortwave heating rates may not exceed the absolute value of the longwave cooling rates. Ballard et al. (1991) in their modeling study of sea fog off the coast of Scotland limited shortwave heating to never exceed the magnitude of longwave cooling, since longwave cooling is the dominant radiative forcing term at cloud top. The literature indicates that the maximum shortwave heating rates in low-level stratocumulus are usually some fraction of the absolute value of the longwave cooling: (shortwave heating rate)/abs(longwave cooling rate) = 1/6 (Oliver et al. 1978), 1/4 (Stephens 1978), and 1/3 (Duynkerke and Hignett 1993). For midlevel water clouds, Hu and Stamnes (1993) found the fraction to be 1/10.

Slingo (1989) and Slingo et al. (1989) showed that simpler broadband radiation schemes such as that used in MM5 tend to overestimate shortwave absorption by cloud as compared to more realistic schemes with four or more wavelength bands. There is also a tendency to underestimate the longwave cooling from low-level stratus because of limited vertical resolution in the models. Thus, for this study, the shortwave heating rate within clouds was constrained to not exceed one-third the magnitude of the longwave cooling. While this approach corrects the net temperature tendency by introducing a compensating artificial constraint, it is an acceptable step for a 3D model where vertical resolution is somewhat limited.

Background minimum vertical diffusion was also found to be an important parameter for accurate prediction of the vertical structure of the MBL and marine stratus. As with many turbulence schemes, the Blackadar PBL imposes a small background value for vertical diffusion to ensure numerical stability and vertical coupling between model layers during stable conditions. The model's ability to simulate the large vertical temperature and moisture gradients commonly found near the top of the MBL is quite sensitive to this background value of vertical diffusion. We found that the default value for background vertical diffusion in MM5 (1.0 $m^2\ s^{-1}$) was too large and unrealistically weakened the vertical gradients of temperature and moisture at the top of the MBL. Therefore, the background value was reduced to 0.01 $m^2\ s^{-1}$ to preserve realistic vertical gradients associated with the MBL.

3. Model initialization

a. Static initialization

A static initialization of the MM5 is performed by blending observations into first-guess global analyses produced by the National Centers for Environmental Prediction (NCEP). The first-guess analyses are available every 12 h and include virtual temperature, geopotential height, u and v wind components, and relative humidity on mandatory levels on a 2.5° × 2.5° latitude–longitude grid. Archived daily sea surface temperature analyses available from the U.S. Navy are horizontally interpolated to the 36-km coarse grid mesh (CGM). The NCEP analyses are also interpolated to the CGM on mandatory pressure levels plus the following supplementary analysis levels: 975, 950, 925, 900, 875, 800, 750, 650, 600, and 550 hPa. These first-guess fields are then updated with surface and upper-air observations using a modified successive-correction scheme (Benjamin and Seaman 1985) applied at the surface, and to the mandatory and supplementary analysis pressure levels. In this case, the standard analysis scheme is modified in the coastal zone so that coastal temperature and moisture observations are not used uniformly in the onshore and offshore directions, because these observations are generally unrepresentative of both regimes simultaneously.

The modified scheme first analyzes the wind direction below 850 hPa at coastal stations to determine whether onshore or offshore flow exists. The thermal and moisture data are then applied only in that portion of the standard area of influence (a modified ellipse) that represents the source region of the flow. For example, if the flow is onshore, a coastal observation is only applied within the area of influence in the offshore direction. This approach is important to preserve the low-level baroclinity characteristic of the coastal zone. Lateral boundary conditions for the 36-km grid are specified every 12 h from these data-enhanced NCEP analyses using a boundary relaxation technique on the outermost five rows and columns (Grell et al. 1994).

The 12-km fine grid mesh (FGM, Fig. 1) is statically initialized by horizontally interpolating the surface and upper-air analyses on pressure levels from the CGM to the FGM domain, followed by a vertical interpolation to the FGM sigma surfaces (the FGM has higher-resolution terrain and land use information than the CGM). Lateral boundary conditions for the FGM are supplied by the CGM at each advective time step in a two-way interactive nested-grid procedure (Grell et al. 1994).

b. Dynamic initialization

For a dynamic initialization, data are assimilated into the model solution during, for example, a 12-h pre-

forecast period. This four-dimensional data assimilation (FDDA) approach is designed to improve model initial conditions by allowing the mass and wind fields to come into some degree of dynamic balance, while the model ''spins up'' mesoscale structures consistent with grid resolution (e.g., small-scale circulations, clouds, precipitation). Two different dynamic initialization techniques are used in this study and are described below.

1) Observation nudging FDDA

A simple method to dynamically initialize a numerical model is to assimilate data by relaxing or ''nudging'' the model solution toward observations during the preforecast period. Two types of data can be assimilated into the MM5: 1) gridded analyses temporally interpolated at each model time step, and 2) individual observations distributed nonuniformly in space and time. These two techniques are known as ''analysis nudging'' and ''obs nudging,'' respectively (Stauffer and Seaman 1990, 1994; Stauffer et al. 1991).

Analysis nudging is not used in this study because of the comparatively poor quality of the MBL structure in the NCEP analyses in the offshore data-void regions. Observation nudging is used here to assimilate data available from a variety of observing platforms over the land during a 12-h preforecast initialization period. After the preforecast period (−12 to 0 h), the model simulation continues without any data assimilation for an additional 24-h ''free forecast'' (0–24 h).

The special data used here were collected under the direction of the California Air Resources Board and the Joint Powers Agency in two simultaneous coordinated field programs: the San Joaquin Valley Air Quality Study (SJVAQS) and the Atmospheric Utility Signatures, Predictions and Experiments (AUSPEX). These programs were designed to investigate ozone emissions, transport, and air chemistry under the subsuquent SJVAQS/AUSPEX Regional Modeling Adaptation Project (SARMAP). The SARMAP meteorological data include 27 rawinsondes with mass and wind data at 3- or 6-h intervals, and hourly wind data from 12 Doppler acoustic sounders and seven radar profilers distributed throughout the San Joaquin Valley and the Coast Ranges. Furthermore, wind data from 159 surface observation sites in the same region are available for assimilation.

To save computational time, observations are vertically interpolated to the model sigma layers in a preprocessing step, and nudging corrections (model minus observed values) are recomputed every other CGM time step (every six FGM time steps). The upper-air (surface) observations influence the model solution within 2 h (1 h) of the observation times, and a modified Cressman function is used to define the horizontal weighting, as described in Stauffer and Seaman (1994). Observations in mountain (valley) regions have a much reduced impact in valley (mountain) regions where they are expected to be less representative. The horizontal radius of influence for obs nudging of upper-air data is 100 km at the surface and increases linearly with decreasing pressure to 200 km at 500 hPa. Above the 500-hPa level, the radius of influence is 200 km. The vertical radius of influence is defined to be very small, so that the obs-nudging corrections are applied quasi-horzontally at the height levels to which the observations have been interpolated. Surface wind corrections are applied horizontally with a radius of influence of 50 km and vertically with decreasing weight through the lowest 200 m of the atmosphere.

2) Marine boundary layer initialization

The goal of the marine boundary layer initialization (MBLI) scheme is to establish a more realistic MBL in the data-sparse coastal zone and offshore regions than is possible by conventional initialization techniques. The basis of the MBLI is a climatology for inversion-base height presented by Neiburger (1960) and used as a target toward which the model is continuously nudged during the preforecast period (Fig. 2). The inversion base also typically defines the top of the marine stratus clouds, which are persistent over the northeast Pacific in summer and significantly affect marine-layer stability. Thus, both model temperature and moisture fields over the ocean are relaxed toward profiles constructed from Neiburger's inversion-base climatology. Seven user-defined parameters can be specified according to the meteorology of the case (see Fig. 3). It is important to note that the MBLI scheme can be used with any inversion-base climatology, analysis, or conceptual model. This work is intended to demonstrate proof of concept for the MBLI approach.

The inversion base is used here to define the depth of the MBL. The climatological data described by Neiburger (Fig. 2) are used to specify a target depth for the marine layer, represented by the height of the nearest computational sigma level in MM5. First, target profiles of temperature and mixing ratio are constructed for each oceanic and coastal zone grid point at each time step during a 12-h preforecast period.

1) Starting at the surface layer (lowest computational layer), the target temperature is set equal to the current time step model temperature so that the thermodynamic balance between the ocean surface and the lowest computational layer is not disturbed.
2) Target temperatures for model layers above the surface layer are determined according to two user-defined lapse rates, RLAP1 and RLAP2, and a user-defined PBL fraction, PBLF. The PBL fraction parameter specifies the ratio of the depths of the layers to which RLAP1 and RLAP2 are applied (see Fig. 3). This allows the user to specify the depth and lapse rates of two layers within the MBL. Observational studies show that the MBL often has a steep-

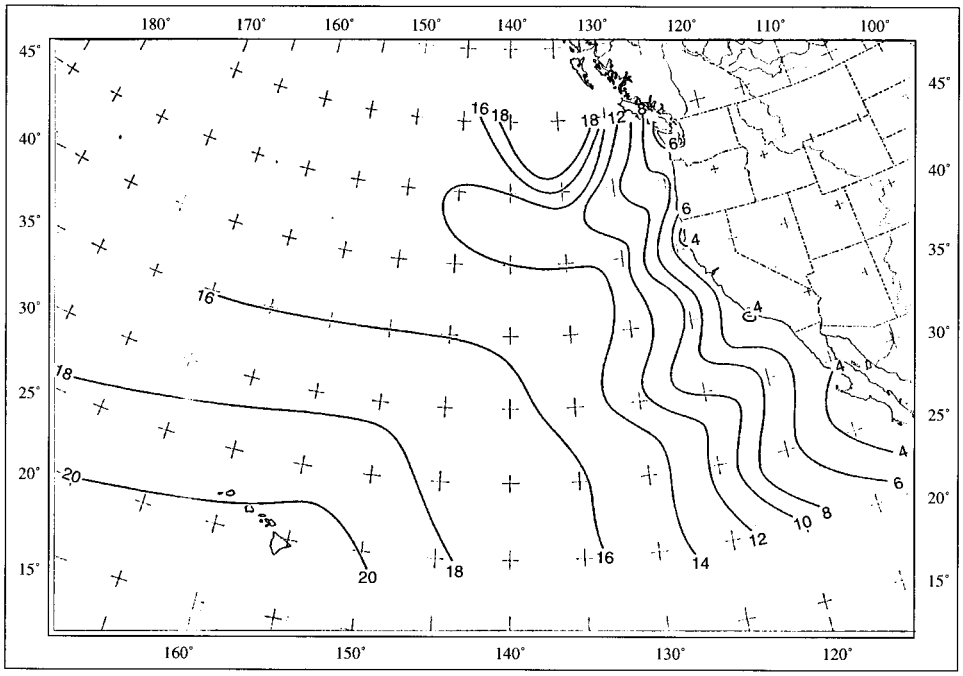

FIG. 2. Observed climatological height of inversion base in summer over the northeast Pacific in hundreds of meters (after Neiburger 1960). Contour interval is 200 m.

er lapse rate just above the ocean surface than near the inversion base (Nicholls and Leighton 1986; Duynkerke et al. 1995). Thus, a bimodal MBL thermal profile is specified. While more complex MBL thermal profiles have been observed (Nicholls and Leighton 1986), a bimodal specification usually is sufficient for assimilating climatological information.

3) Above the top of the climatological MBL, the target temperature is set equal to the current time step MM5 value at the inversion base. This value is also the target temperature for KTRAN transitional layers above the MBL over which the nudging term is gradually removed. That is, model temperatures are nudged to this target profile with full weight (W_{T0}) through the MBL (see Fig. 3a), but the nudging weight decreases linearly (with respect to computational layers) above the inversion base according to KTRAN.
4) Similar to the temperature field, the target moisture profile is set equal to the current time step model mixing ratio in the surface layer to keep the model's surface-layer moisture balance undisturbed.
5) Target mixing ratios for MBL layers above the surface layer are determined according to two user-defined parameters, CLDEPTH and RHMBL (see Fig. 3b). The target cloud base is determined from the height of the climatological inversion base minus the user-defined target cloud depth (CLDEPTH) by assuming that the cloud top coincides with the inversion base. Target mixing ratios below cloud base are then set according to the user-defined value for relative humidity below cloud base (RHMBL) and the current model temperature profile.
6) Target mixing ratios for model layers within the target cloud are calculated by assuming 100% relative humidity using the current model temperatures.
7) Model mixing ratios are nudged to the target profile with full weight (W_{q0}) within the MBL, and with zero weight for all layers above the inversion base.

Note that the target MBL temperature and moisture profiles vary in space and time according to the current time step temperature and mixing ratio in the surface layer during the preforecast. Horizontal weighting of the MBLI nudging terms is uniform over the ocean and reduced inland from the coast. The JCOAST parameter (see Fig. 3c) determines the number of grid points either inland (JCOAST > 0) or offshore (JCOAST < 0) over which the MBLI forcing for temperature and moisture is linearly reduced to zero. For this study, RLAP1 = 9.5°C km^{-1}, RLAP2 = 8.5°C km^{-1}, PBLF = 0.5, KTRAN = 2, CLDEPTH = 300 m, RHMBL = 95%, and JCOAST = 3 (CGM) and 5 (FGM).

4. Experimental design

Six experiments are used to compare the effect of different initialization strategies on the initial conditions and ensuing 24-h forecasts in the coastal zone. An afternoon initialization (0000 UTC) was chosen because preliminary experiments showed that the initialization

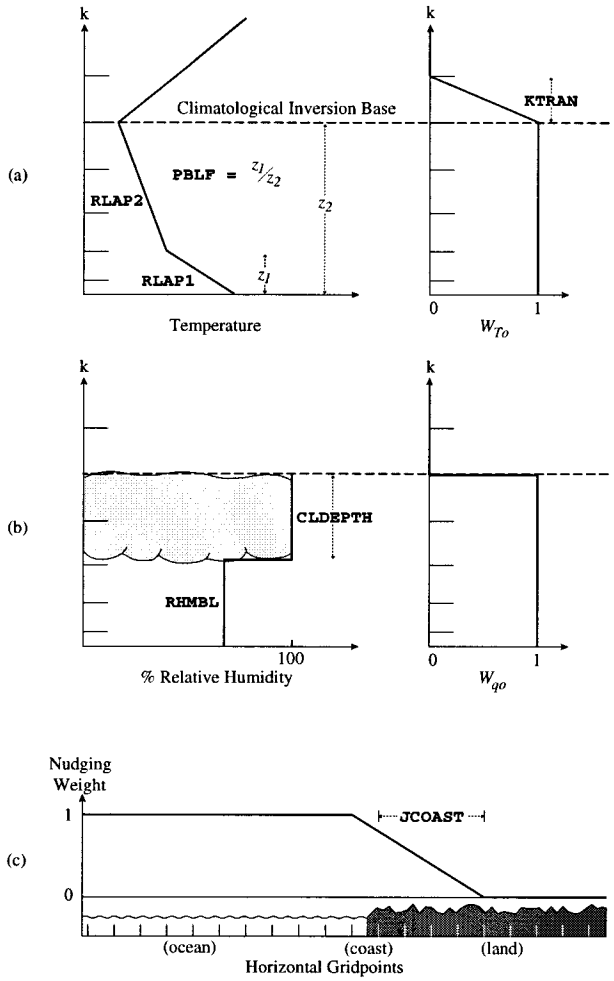

FIG. 3. Schematic diagrams of MBLI user-defined parameters: (a) target thermal profile specifications, (b) target moisture profile specifications, and (c) distribution of horizontal nudging weights in the coastal zone. See text for explanation.

and maintenance of marine-layer stratus in the model was more difficult during the afternoon due to the dissipative effects of the sun on cloud water. If a realistic MBL can be established and maintained during the day, then a morning initialization can be accomplished more easily. A meteorological overview of the case is presented in section 5b.

The goal of these experiments is to produce accurate initial conditions and 24-h ''forecasts'' within the coastal zone. The term forecast is used here to describe the simulation period following either a static initialization (SI) at $t = 0$ h or a dynamic initialization (DI) from $t = -12$ to $t = 0$ h. The forecast period ($t = 0$ to $t = 24$ h) represents a numerical prediction in the operational sense, except that the lateral boundary conditions reflect available observations. All DI techniques in this study are applied during the 12-h period prior to the $t = 0$ h start of the forecast. The nudging terms for all of the DI techniques are reduced linearly in time to zero during the first hour after $t = 0$ h to avoid causing a large adjustment, as could occur when removing the nudging terms suddenly from the model equations.

TABLE 1. Experimental design.

Exp mnemonic	Data assimilation
CNTL	None
BSLN	None
OBSMW	Obs nudging to mass and wind field observations
OBSM	Obs nudging to mass field observations only
MBLI	Marine boundary layer initialization (MBLI)
OBSMBL	OBSMW + MBLI

Table 1 outlines the data assimilation strategies used in this experimental design. First, a 24-h control experiment (CNTL) is performed to establish MM5's forecast skill from a static initialization (no MBLI or FDDA) at 0000 UTC 4 August 1990. Next, a 36-h baseline experiment (BSLN) is performed from a static initialization prescribed 12 h earlier at 1200 UTC 3 August 1990 to allow a value-added comparison with the DI experiments that begin at the same time. Then, DI experiments test four different data assimilation strategies: the first DI experiment (OBSMW) uses obs nudging to assimilate both mass and wind data. The second DI experiment (OBSM) is the same as OBSMW except only mass data are assimilated (temperature and mixing ratio), so that induction effects on the wind field due to assimilation of only mass field data can be identified. The third DI experiment (MBLI) uses only the MBLI scheme to improve the initial conditions. Similar to OBSM, MBLI directly affects only the mass fields while the wind fields are free to adjust to the changing mass fields. All parameters in this application of the MBLI scheme are described in section 3b(2). The fourth DI experiment (OBSMBL) combines the obs nudging for both mass and wind with the MBLI scheme. The goal of OBSMBL is to use the obs nudging to improve initialization where wind and mass observations are available, while the MBLI scheme is used to establish climatological conditions over the ocean where data are not available.

5. Meteorology of the northeast Pacific and case description

a. General discussion of meteorology of the northeast Pacific

The Pacific high pressure ridge exerts a strong influence on the MBL over this region. Low-level winds are divergent and air descends through much of the troposphere. The persistent sinking motion adiabatically compresses and warms the atmosphere above the MBL. When the warm, dry, sinking air beneath the synoptic high meets relatively cool, moist MBL air, a strong temperature inversion forms at the top of the MBL. The inversion is typically 5°–20°C through a 200–500-m

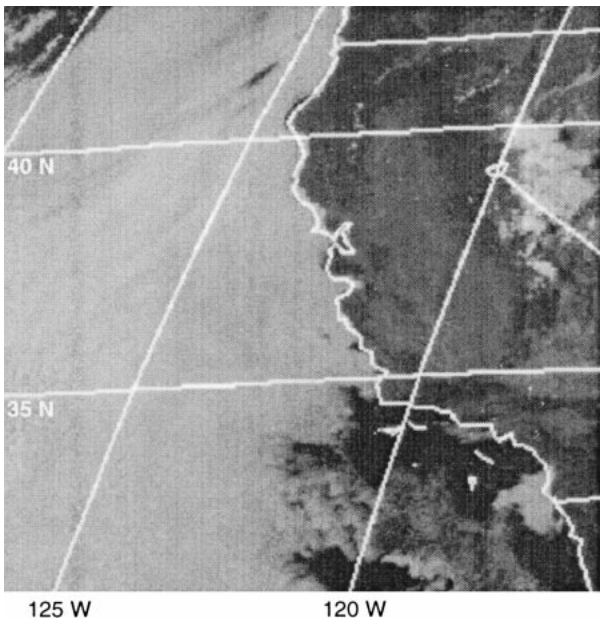

FIG. 4. GOES-West visible satellite image at $t = 0$ h (0000 UTC 4 Aug 1990).

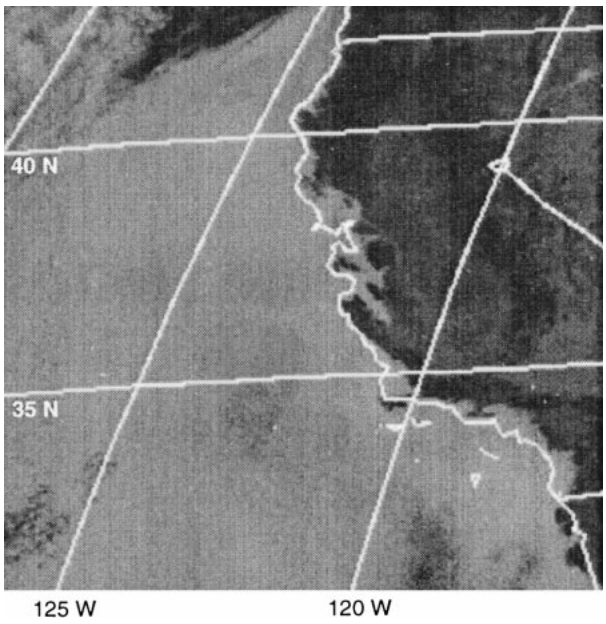

FIG. 5. GOES-West visible satellite image at $t = 15$ h (1500 UTC 4 Aug 1990).

layer (Neiburger 1960) and is especially stong and persistent in the California coastal zone. Farther offshore and farther north, the inversion becomes less prevalent, but is still present more than 50% of the time over much of the northeast Pacific. The position and intensity of the surface high changes little during the summer months, but even small changes in its intensity and position are reflected in the depth and stability of the MBL. When the high intensifies or moves closer to the coast, the inversion at coastal stations strengthens and the depth of the MBL decreases.

Observational studies of the MBL off the west coast of the United States (Neiburger 1960; Brost et al. 1982; Bridger et al. 1993) have shown that the inversion base rises with distance offshore, usually being lowest at the coast. Northerly winds parallel to the coast induce coastal upwelling of cold water and the MBL is usually shallower over the cold coastal waters than over the warmer waters offshore (Elliott and O'Brian 1977; Beardsley et al. 1987), owing to smaller positive buoyancy fluxes from the ocean surface. In the afternoon, the sea breeze increases low-level subsidence in the coastal zone, which also contributes to a lower inversion base near the coast. Neiburger showed that the depth of the MBL increases from ~500 m at San Francisco to ~2000 m at Honolulu (see Fig. 2).

Marine stratus is a common feature over the northeast Pacific in the summertime. For example, Simon (1977) found that the overall mean low-level cloud cover off the coast of California was 55.5% to 132°W during the summer of 1975. The diurnal variation in cloud over the same region was about 18% with maximum cloud cover at 0745 Pacific standard time (PST) and minimum cloud cover at 1345 PST. Marine boundary layer clouds often advance inland at night, sometimes producing coastal fog, and retreat offshore during the late morning or early afternoon (Byers 1930; Edinger 1963). With cloud tops at the inversion base, the stratus clouds should also be expected to exhibit an offshore-sloped structure during the summer.

b. Case description

The case chosen for this study, 1200 UTC 3 August–0000 UTC 5 August 1990, is representative of the typical summertime meteorology in the northeast Pacific. Figures 4 and 5 show *Geostationary Operational Environmental Satellite-7* (*GOES-7*) visible imagery valid at $t = 0$ h (0000 UTC 4 Aug) and $t = 15$ h (1500 UTC 4 Aug), respectively. The cloud cover over the region exhibits the typical diurnal trend reported by Simon and others: cloud clearing in coastal regions during the day (Fig. 4) and cloud development during the night (Fig. 5). The clearing is especially noticable in the California Bight south of 35°N.

Figure 6 shows the 500-hPa height field at the beginning of the period. A longwave trough along 145°W is flanked by two ridges. Through the period, the trough moves east by a few degrees of longitude and the ridge just off the West Coast moves onshore and inland. MBL depths as inferred from coastal rawinsondes decrease by a few tens to a hundred meters through the period in response to the increased subsidence under the advancing ridge. Figure 7 shows sea level pressure at the beginning of the period. Sprawling surface high pressure across the northeast Pacific helps create a significant

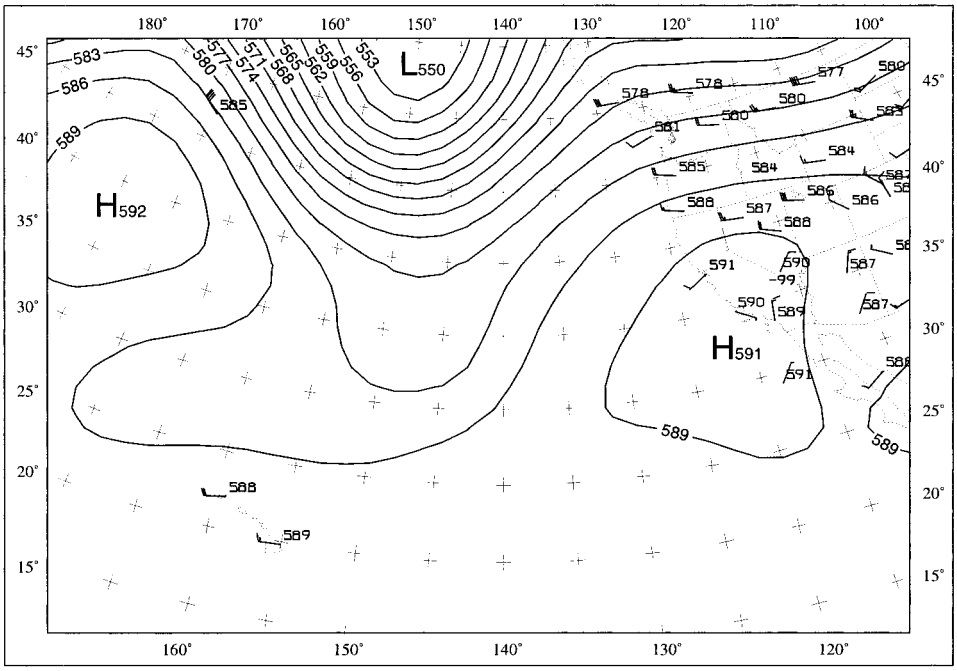

FIG. 6. Analysis of 500-hPa heights (dam) at 1200 UTC 3 Aug 1990 from NCEP spectral initial conditions. Height contour is 3 dam. Observed winds (full barb = 5 m s^{-1}) and heights.

pressure gradient and northerly flow in the California coastal zone. The surface pressure pattern is quasi-steady through the period with the largest changes occurring over land in response to the diurnal heating cycle.

6. Results of the numerical experiments

Vertical cross sections of potential temperature and cloud water are presented first to illustrate the effect of dynamic initialization on the vertical structure of the

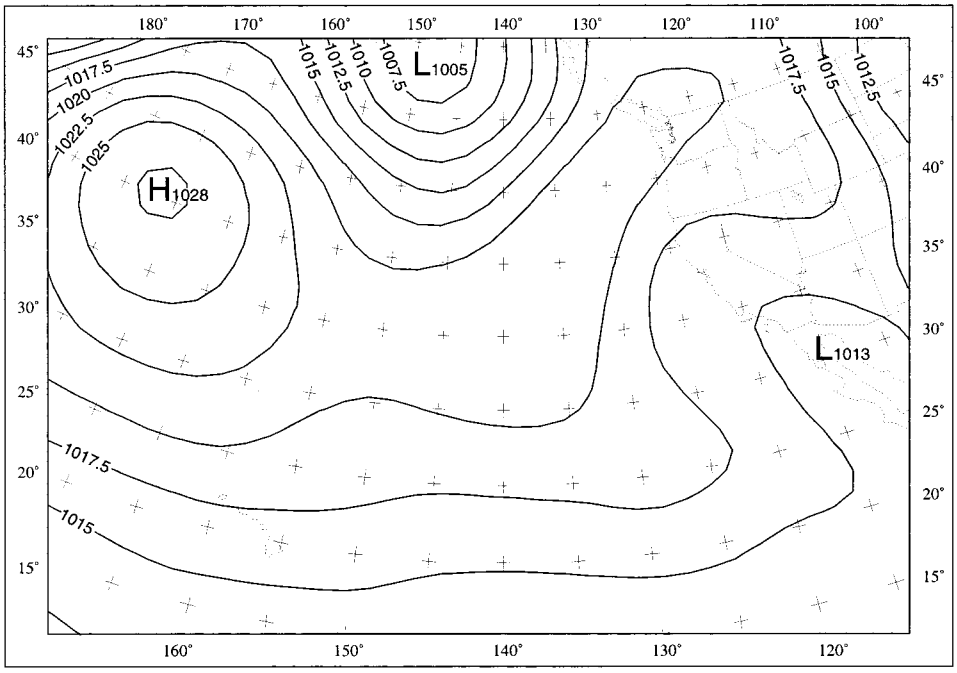

FIG. 7. Analysis of sea level pressure (hPa) at 1200 UTC 3 Aug 1990 from NCEP spectral initial conditions. Contour interval is 2.5 hPa.

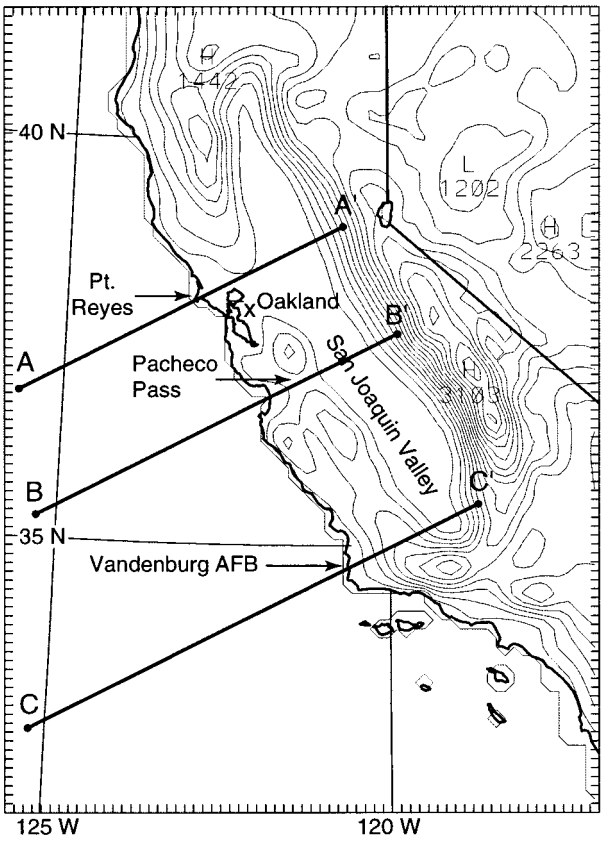

FIG. 8. The 12-km grid with cross-section locators. The terrain contour interval is 200 m.

MBL offshore. Then, visible satellite images are used to qualitatively verify cloud cover forecasts over the northeast Pacific. Finally, quantitative verification of the model forecasts in the coastal zone is based on the standard and special rawinsonde observations collected during the SARMAP field study program. Six-hourly coastal soundings available at Point Reyes, Oakland, and Vandenburg, California (see Fig. 8), are the principle data used to verify the forecasts. Ten parameters derived from these coastal soundings (including MBL depth, and temperature and moisture gradients at the top of the boundary layer) are tabulated and compared with observed values to quantify the effectiveness of each initialization method.

a. Cross-section analysis

The structure of the MBL is analyzed using cross sections A, B, and C defined in Fig. 8. Many improvements in the initial conditions and forecasts due to the data assimilation are illustrated clearly by these cross sections oriented perpendicular to the coast. Because upstream conditions tend to dominate the coastal zone forecasts in experiment BSLN and the obs-nudging experiments (OBSMW and OBSM), the skill of their initializations and forecasts after 6 h are mostly similar. Therefore, cross sections are presented only for experiments BSLN and OBSMBL to highlight the effects of FDDA on the forecasts.

1) INITIAL CONDITIONS

Figure 9 shows cross sections at $t = 0$ h from BSLN after 12 h of model preforecast integration. The cross sections show potential temperature (θ, interval 2 K, thin contours) and cloud boundary (0.05 g kg^{-1} cloud water mixing ratio isopleth, thick contours). These cross sections correspond to 0000 UTC 4 August 1990 [1700 Pacific daylight time (PDT)], the hottest part of the day. Notice the transition from a shallow cool, moist boundary layer offshore to a deep (>1 km), well-mixed, dry and warm PBL over the Central (San Joaquin) Valley of California. Clouds have developed in BSLN but they are generally surface based (Figs. 9a,b) and the temperature inversion is quite weak, especially in the south and west (Fig. 9c).

Figure 10 shows results at $t = 0$ h from OBSMBL. Among the many differences evident between the cross sections from OBSMBL and BSLN at this time, the use of obs nudging and climatological information via the MBLI

- creates a MBL two to three times deeper than in BSLN;
- roughly doubles the vertical temperature gradient through the marine inversion layer;
- establishes an *elevated* stratus deck, except in northern coastal regions;
- establishes a sloping MBL height that increases with distance from the coast (following Neiburger's climatology); and
- reduces mixing heights in the San Joaquin Valley by 10%–20% via inflow of cooler more stable air from the MBL offshore.

Thus, assimilation of observations and climatological information greatly improves the vertical and horizontal structure of the MBL offshore as well as in the coastal zone in the initial conditions (in the climatological sense, at least). A detailed quantitative verification against coastal observations is presented in section 6c.

2) MODEL FORECASTS

Figures 11 and 12 show cross sections at $t = 12$ h for BSLN and OBSMBL, respectively. These cross sections are valid at 1200 UTC 4 August 1990 (0500 PDT), about 1 h before sunrise. Many of the differences described above between BSLN and OBSMBL at $t = 0$ h are still evident. Longwave cloud-top cooling through the night has increased the horizontal coverage of clouds for both BSLN and OBSMBL. The shallow MBL has grown very little in BSLN, while OBSMBL maintains the MBL structure established in the initial conditions.

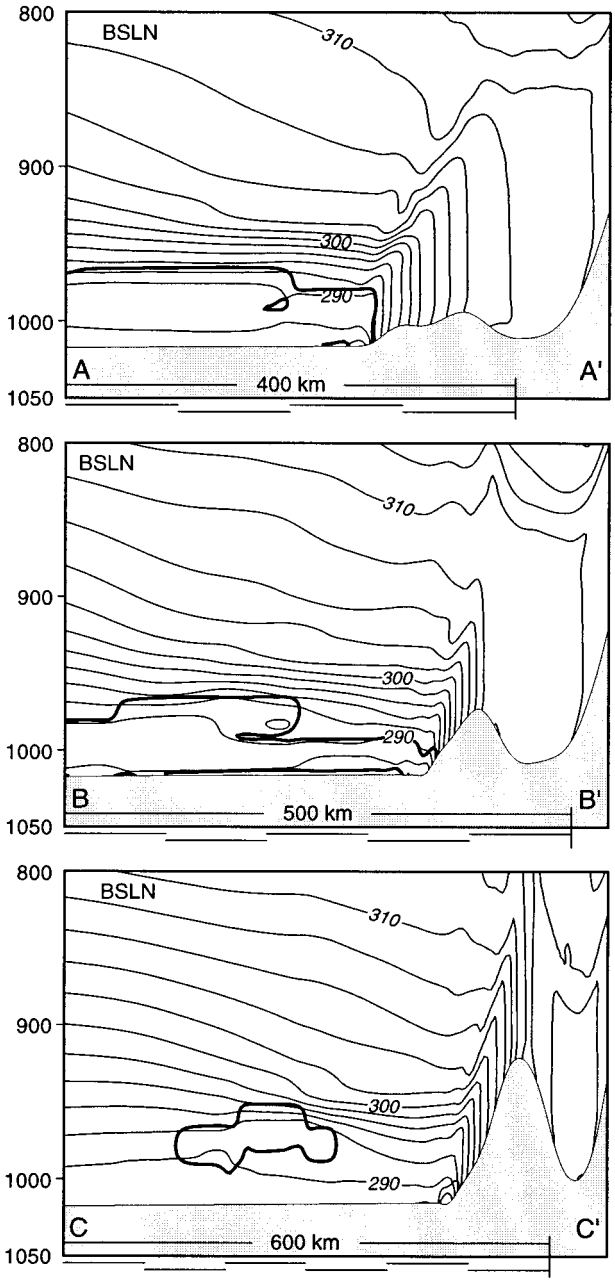

FIG. 9. Simulated cross sections of potential temperature (thin, every 2 K) and cloud boundary (thick, cloud water mixing ratio = 0.05 g kg^{-1}) at t = 0 h (0000 UTC 4 Aug 1990) for three cross sections from expt BSLN. See Fig. 8 for location of cross sections.

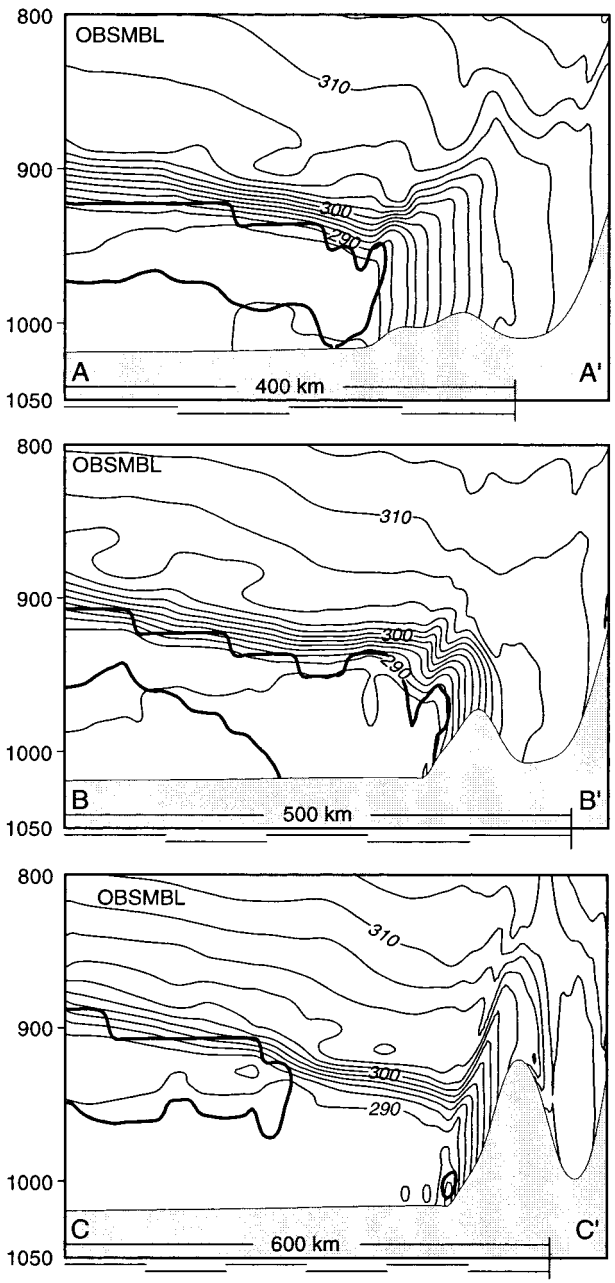

FIG. 10. Same as Fig. 9 but from the OBSMBL expt.

Figures 13 and 14 show the 24-h forecast cross sections valid at 0000 UTC 5 August 1990 for BSLN and OBSMBL, respectively. Portions of the stratocumulus cloud deck offshore have dissipated under the effect of strong solar heating in both experiments consistent with available satellite imagery (not shown). Inland from San Francisco Bay, the mixing heights over the Central California Valley in experiment OBSMBL are lower and the temperature on the floor of the valley is cooler in OBSMBL than in BSLN (compare 310-K contours in Figs. 13a and 14a). Meanwhile, the MBL is deeper and the marine inversion is stronger in the OBSMBL cross sections than in BSLN.

Using the three coastal soundings, we also performed a point verification of boundary layer depth. Figure 15 shows the temporal evolution of the PBL depth at Point Reyes for all six experiments (dashed lines) versus the observed conditions (thick solid line). Results for Point

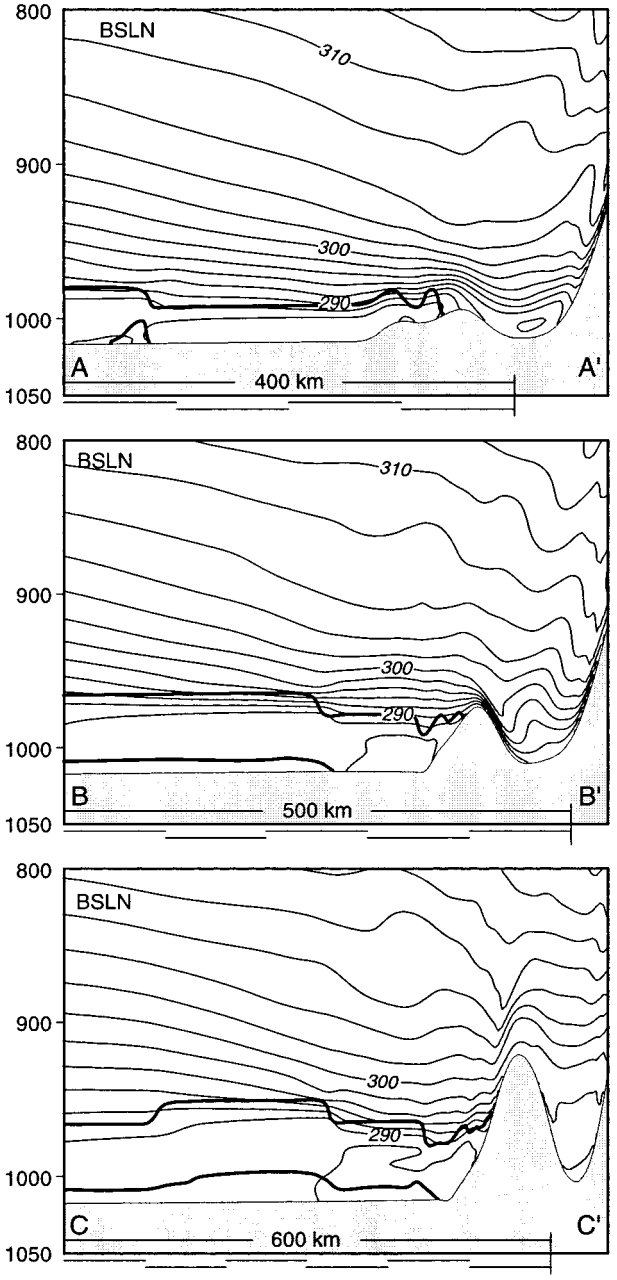

FIG. 11. Same as Fig. 9 but for $t = 12$ h forecast (1200 UTC 4 Aug 1990).

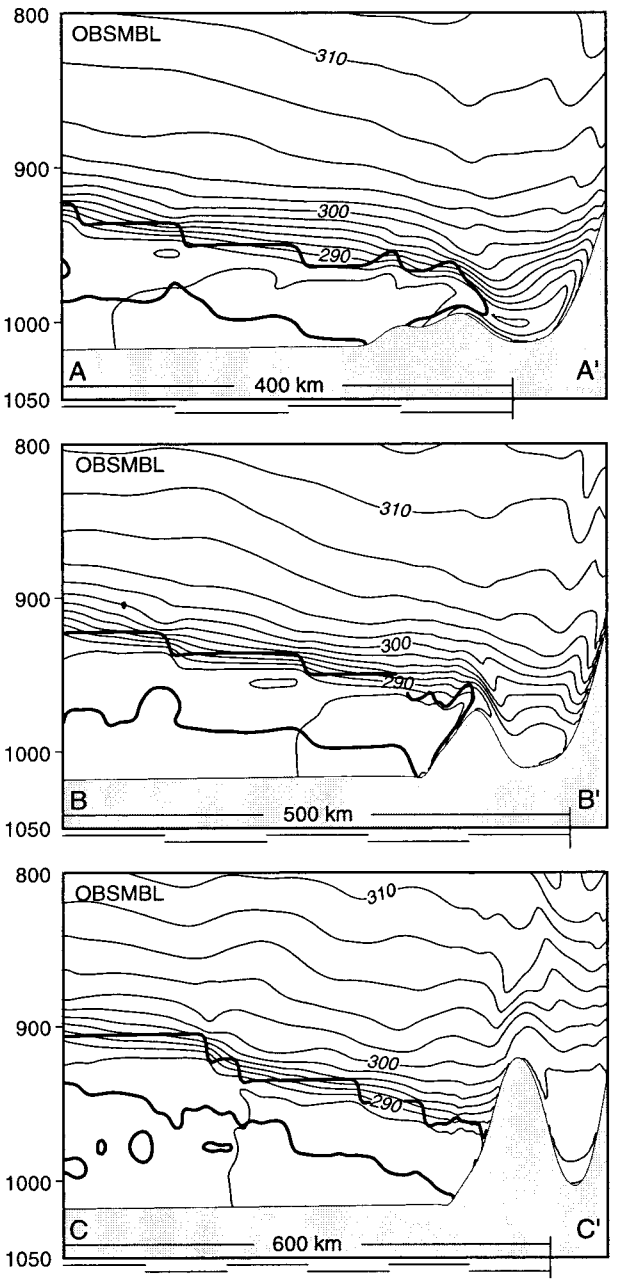

FIG. 12. Same as Fig. 11 but from the OBSMBL expt.

Reyes are fairly representative of all three coastal stations. Experiments CNTL and BSLN fail to produce a boundary layer deeper than ~100 m, while those experiments that used climatological information, MBLI and OBSMBL, were able to maintain the deepest boundary layers through the 24-h forecast period. Although the experiments using only obs nudging (OBSMW and OBSM) produce a reasonably deep boundary layer at the initial time ($t = 0$ h), they fail to maintain it after only 6–12 h. This occurs because the obs nudging improves the initial conditions in the vicinity of the observations. However, once poor quality offshore conditions advect into the coastal zone from the upstream data-void region, the beneficial effect of these observations in the initial conditions is lost.

The evolution of the boundary layer and cross sections show that the OBSMBL forecasts for MBL structure are the most accurate of all the experiements. Thus, there is a clear advantage to using climatology via MBLI to initialize mesoscale models off the west coast of the United States during the summertime.

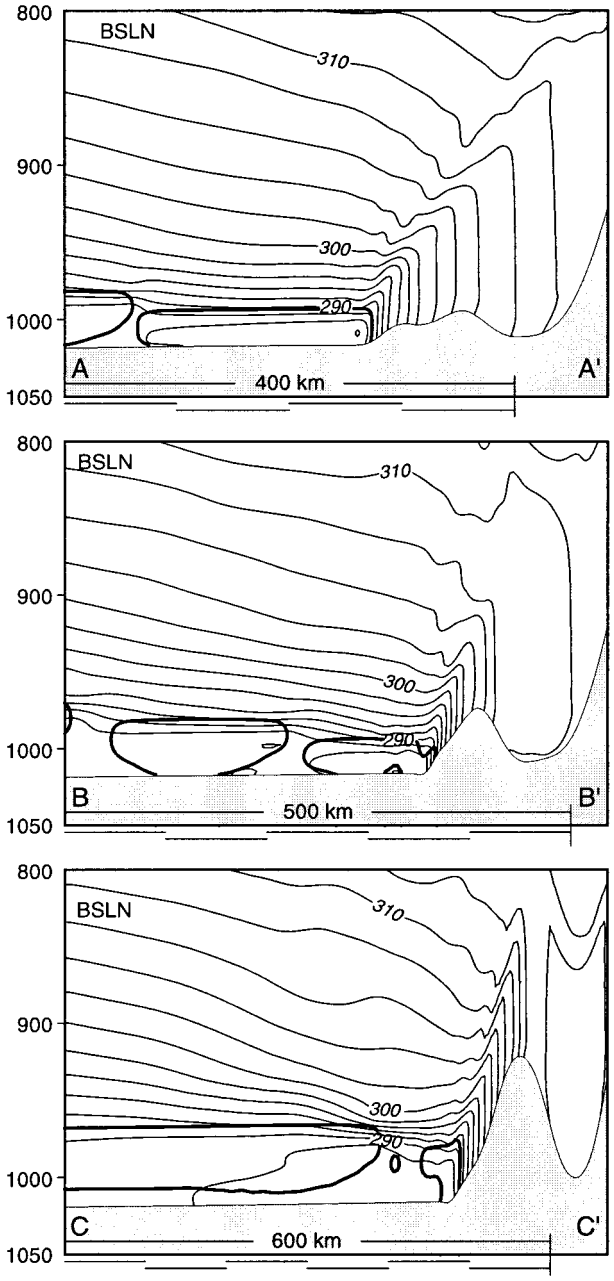

FIG. 13. Same as Fig. 9 but for $t = 24$ h forecast (0000 UTC 5 Aug 1990).

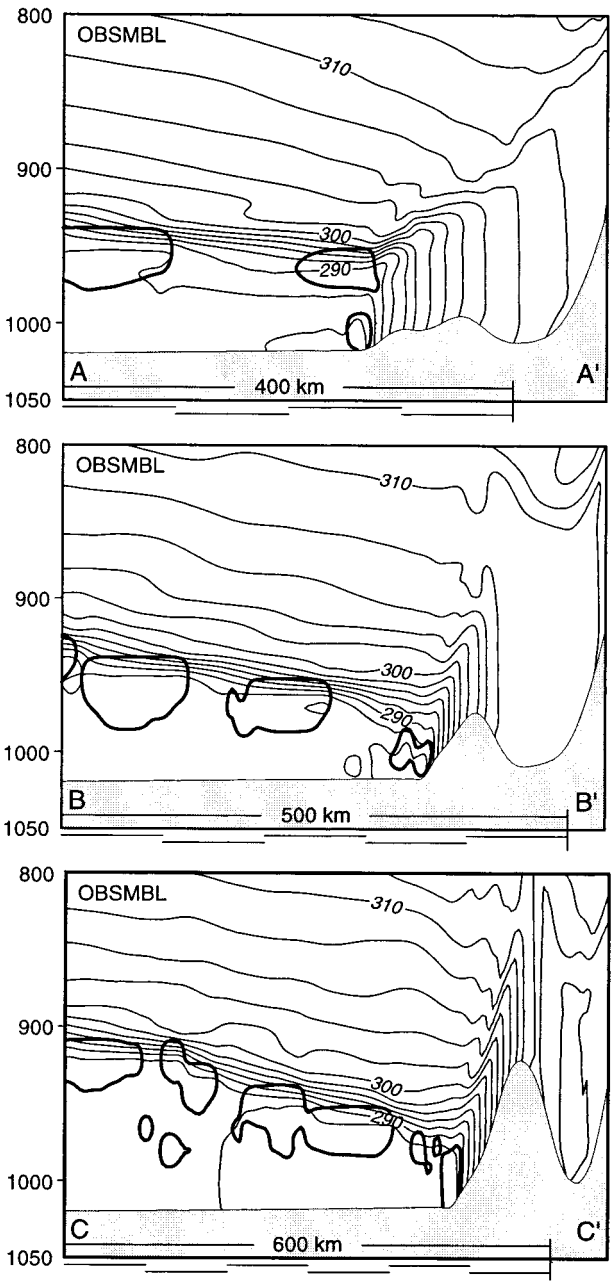

FIG. 14. Same as Fig. 13 but from the OBSMBL expt.

b. Satellite cloud verification

In this section, the *GOES-7* visible imagery is used to validate initial-condition and forecast cloud cover from BSLN and OBSMBL.

1) INITIAL CONDITIONS

Figure 16 shows model-simulated cloud-base heights on the 12-km grid at $t = 0$ h for BSLN and OBSMBL. Regions with cloud water mixing ratios exceeding 0.05 g kg^{-1} are shaded and numbered according to their cloud-base height above ground level: 1 = lowest layer (30 m), 2 = 106 m, 3 = 207 m, 4 = 323 m, 5 = 450 m, 6 = 578 m, 7 = 707 m, and 8 = 838 m. See Fig. 4 for the corresponding *GOES-7* visible satellite image.

There are two striking differences between the cloud cover in BSLN versus OBSMBL at $t = 0$ h. The areal extent of the cloud deck is much greater in OBSMBL (better agreement with the GOES image in Fig. 4), and the cloud-base heights are up to 400 m higher (better agreement with Neiburger's climatology in Fig. 2). The

cloud-base heights in OBSMBL increase with distance from the coast and from north to south (again, consistent with Neiburger's climatology). Note that in OBSMBL regions west of the southern California Bight are cloud free out as far as ~123°W, even though the settings of the MBLI parameters are designed to establish stratus clouds everywhere over the ocean. The presence of a cloud-free region after applying the MBLI for 12 h indicates that the technique does not completely overwhelm the model's dynamics, which includes subsidence induced in the synoptic ridge and the coastal sea breeze. Without the assimilation of any specific knowledge of the observed cloud distribution, the combination of obs nudging and the MBLI scheme produced a very realistic cloud distribution at the initial time.

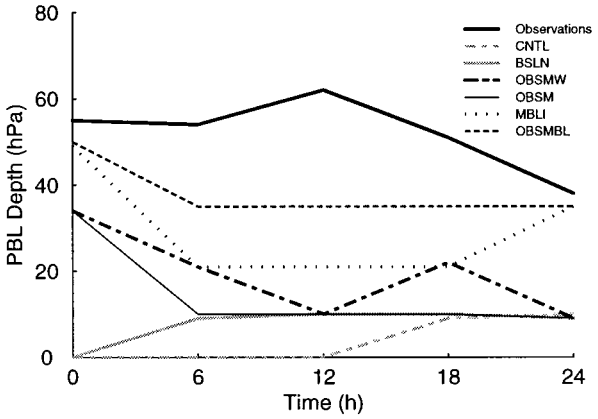

FIG. 15. Temporal evolution of PBL depth (hPa) at Point Reyes, CA, by experiment.

2) MODEL FORECASTS

Figure 17 shows forecasts of cloud-base heights at $t = 12$ h for BSLN and OBSMBL. See Fig. 5 for the corresponding *GOES-7* visible satellite image. The GOES visible image at 1500 UTC is the first available image with useful data after sunrise. As seen in the cross sections, cloud cover increased in both BSLN and OBSMBL through the evening. Notice that fog and low clouds around San Francisco Bay and Monterey Bay are resolved and correctly forecasted on the 12-km grid in both BSLN and OBSMBL. The areal extent of the cloud cover in BSLN and OBSMBL is essentially the same, and in very good agreement with the GOES image. But as at the initial time, the cloud-base heights in OBSMBL (Fig. 17b) are as much as 400–500 m higher, which climatology indicates is likely to be more realistic.

The 24-h forecasts of cloud cover for both experiments are quite similar to each other in areal extent (not shown). Both model forecasts failed to predict some observed cloud-free regions off the West Coast at this time, though much of the oceanic region is covered by low status. The cloud-free regions include most of the California Bight and a clear band about 150 km wide, parallel to the central and southen California coastline, and located 300 km offshore. OBSMBL cloud-base heights, however, are still up to 300 m higher than those in BSLN. This shows that the impact of initializing from Neiburger's climatology persists through the end of a 24-h forecast. Without these improved initial conditions, the MM5 has difficulty generating a realistic MBL structure in this stable environment even after 24 h. In summary, the 24-h cloud-cover forecasts in both experiments are reasonable, but show gradually declining skill, while forecast cloud-base heights are very slow to develop realistic values without the MBLI.

c. Sounding verification

The following 10 parameters derived from coastal soundings were chosen to quantify forecast skill in the coastal zone: PBL depth (hPa), change in temperature through the inversion layer (°C), temperature gradient through the inversion layer (°C hPa^{-1}), change in water vapor mixing ratio through the inversion layer (g kg^{-1}), water vapor mixing ratio gradient through the inversion layer (g kg^{-1} hPa^{-1}), surface temperature (°C), surface wind direction (°), surface wind speed (m s^{-1}), mean PBL dewpoint depression (°C), and mean water vapor mixing ratio in the 800–900-hPa layer (g kg^{-1}).

These 10 parameters were computed from observed soundings and all six model experiments at the three coastal upper-air stations (Point Reyes, Oakland, and Vandenburg) every 6 h through the 24-h forecast period (i.e., 0000, 0600, 1200, 1800 UTC 4 Aug 1990 and 0000 UTC 5 Aug 1990). Table 2 shows the average observed values for each parameter at these coastal stations, along with the model error (model minus observed) for each experiment averaged over the five verification times.

The first three parameters in Table 2 (PBL depth, DT, and $-dT/dP$) are quite sensitive to the initialization method with errors ranging from 3% to 96%. For all stations and experiments, the forecast boundary layer is too shallow. The PBL depth errors tend to be smaller at Oakland than at Point Reyes for CNTL and BSLN because Oakland is farther inland and not influenced as strongly by the cool marine air that inhibits boundary layer growth. Compared to CNTL and BSLN, however, the PBL depth error is reduced significantly for experiments that use obs nudging (OBSMW 29% and OBSM 29%), and is reduced further for those experiments that use offshore climatological information (MBLI 38% and OBSMBL 65%). The cool ocean water off the California coast creates much smaller surface buoyancy fluxes than are typical over land. Preliminary results (not shown) indicated that, without data assimilation, establishing an MBL of considerable depth can take 24–48 h of model integration.

The change in temperature through the inversion layer, DT (Table 2, column 2), and the temperature gradient,

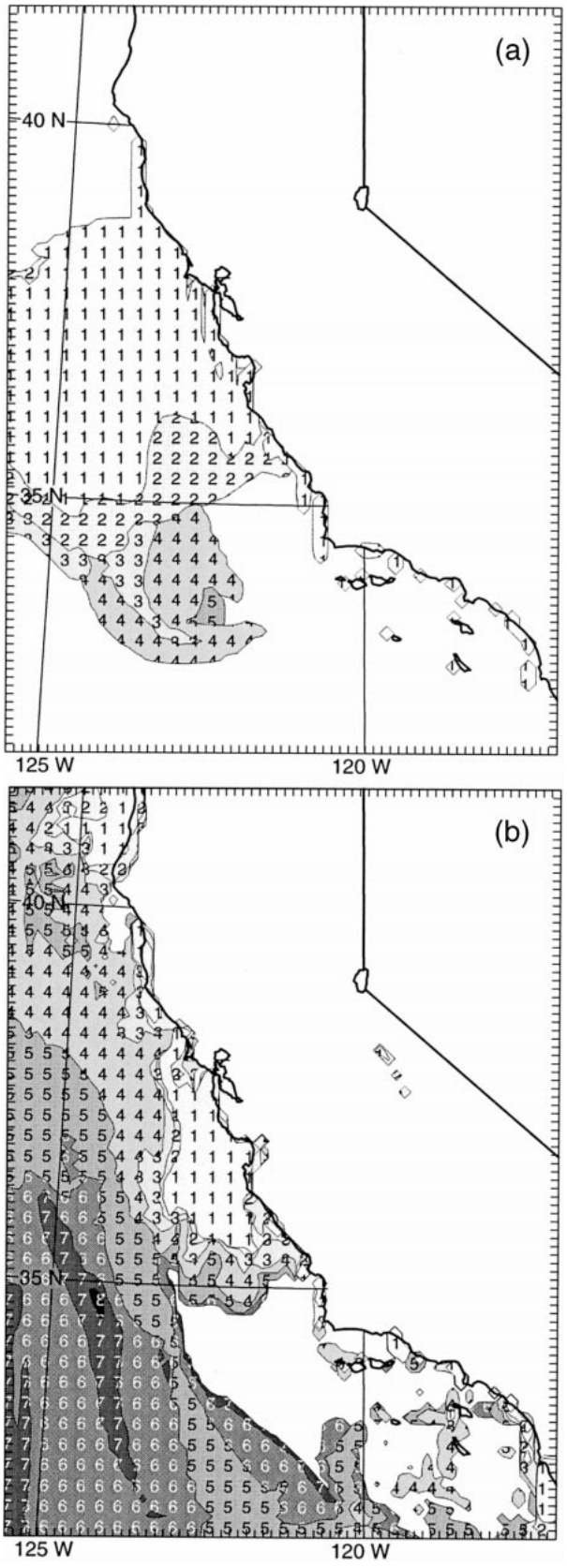

$-dT/dP$ (Table 2, column 3), are closely related to the PBL depth. However, the model still underforecasts the temperature gradients through the inversion layer, despite improvements in PBL depth due to FDDA and the MBLI. Additional MBLI experiments in which the vertical resolution was increased to 55 layers (not shown) demonstrate that greater (more realistic) vertical temperature gradients can form and be maintained in the model. For example, temperature gradients simulated within the marine inversion layer near San Nicolas Island were increased by 100%–200% by tripling the model vertical resolution in this layer (900–950 hPa). This result is largely due to the strong dependence of the relevent model physics, such as radiation and explicit cloud moisture, to layer thickness.

The moisture gradients at the top of the PBL, dQ, and $-dQ/dP$ (Table 2, columns 4 and 5) also benefit from improvements in the PBL depth, but to a lesser extent than for temperature. As with temperature, the moisture gradients are also underpredicted (i.e., inversion layer too moist) in these 30-layer experiments. The predicted moisture gradients reach at best one-half of the observed values and are usually much less. Increasing the vertical resolution to 55 layers allows much stronger vertical moisture gradients to develop (not shown).

For the next four parameters describing surface conditions in the boundary layer (Tsfc, WDIR, WSPD, TDDAVE), there appears to be no large or systematic performance pattern among the six experiments (Table 2, columns 6–9). Several patterns are identifiable from MBLI and OBSMBL, however. In experiments that use the MBLI scheme, average surface temperature is slightly cooler (by 0.1°–1.0°C), wind speed is higher (by 1–2 m s^{-1}), and the PBL is more moist (by 0.1–0.4 g kg^{-1}) at the two stations having the greatest ocean exposure, Point Reyes and Vandenburg. In general, the forecast accuracy of these parameters is degraded slightly in this case, but the results are consistent with the climatological information used in the MBLI scheme.

Evaluation of the errors for all parameters and for each experiment produces nearly a thousand individual measures of forecast accuracy in the coastal zone PBL. In order to assess the relative success of the different initialization strategies, the experiments were ranked ordinally according to the forecast error for each parameter at each validation time (1 for smallest error; 6 for largest error). The ordinal rankings for each parameter and for each experiment were averaged over all validation times.

←

FIG. 16. Forecast cloud cover at $t = 0$ h (0000 UTC 4 Aug 1990) from expts (a) BSLN and (b) OBSMBL. Shaded areas represent cloud water mixing ratios greater than 0.05 g kg^{-1}. Over the ocean, height of model layers above sea level are 1 = lowest layer (30 m), 2 = 106 m, 3 = 207 m, 4 = 323 m, 5 = 450 m, 6 = 578 m, 7 = 707 m, and 8 = 838 m.

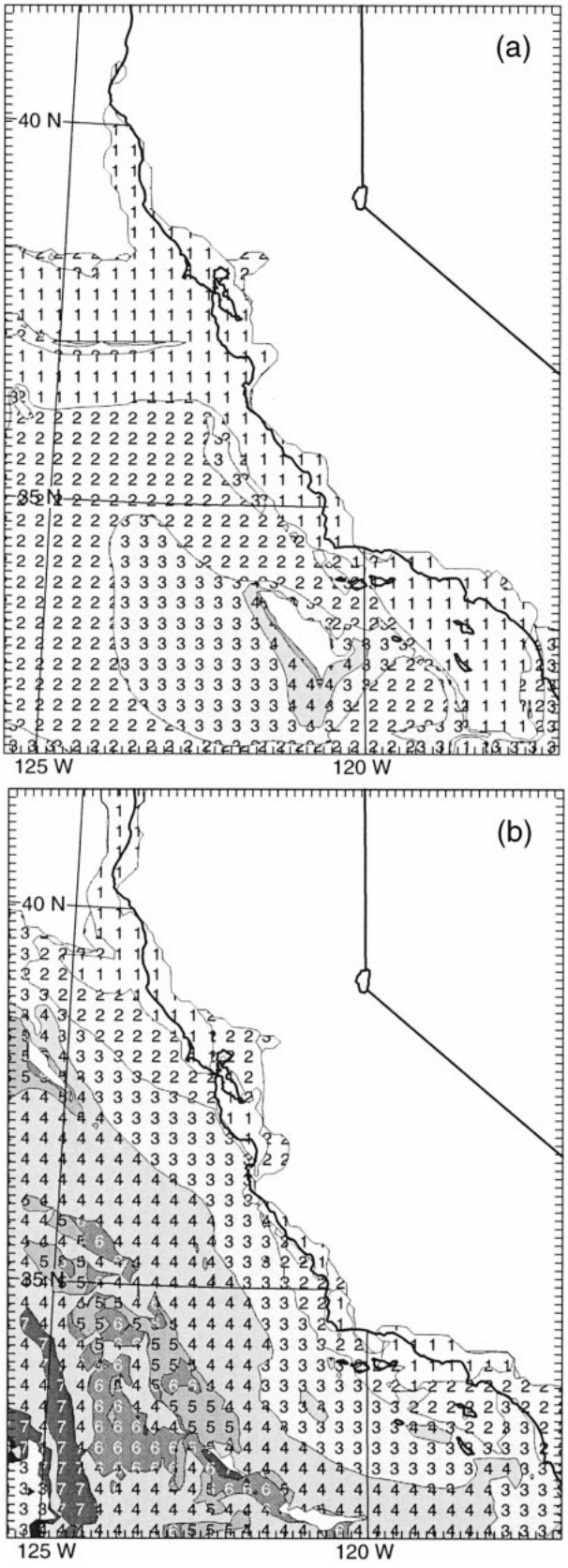

FIG. 17. Same as Fig. 16 but for t = 12 h forecast (1200 UTC 4 Aug 1990).

The results of the ranking are presented in Table 3. Notice that for PBL depth (column 1) there is a clear distinction in skill among the experiments. At all three stations, experiment OBSMBL has the greatest skill (<2), while CNTL has the least (>5). For other parameters, the skill of the experiments is not stratified as clearly. For example, consider average dewpoint depression in the PBL (Table 3, column 9, TDDAVE). The average rank of the experiments at all stations is between 2.6 and 4.8, with no clear pattern among the experiments. This indicates that all experiments had roughly equal skill for forecasting moisture in the PBL. Table 3 demonstrates that, while data assimilation generally improved forecasts of the first five parameters (PBL, DT, $-dT/dP$, DQ, $-dQ/dP$), it did not systematically change the model's forecast skill for the last five parameters (Tsfc, WDIR, WSPD, TDDAVE, QAVE) in this case. Nevertheless, these results suggest that significant improvements can be made to the vertical structure of the MBL (and the coastal zone PBL) in short-range model forecasts without degrading the forecast skill of surface conditions.

The effect of the data assimilation on the forecast of winds and heights at 500 hPa was also investigated, but little effect was found (not shown). This is probably a consequence of the quasi-steady-state conditions in the northeast Pacific during the summer, which allow the NCEP global model to forecast the placement of synoptic-scale features quite well.

To further distill the results obtained thus far, we summed the average ordinal ranks for each experiment over all 10 verification parameters (see Table 3 column 11). The best (minimum) possible summed rank is 10, while the worst (maximum) possible summed rank is 60. From the summed ranks, a pattern begins to emerge that is particularly evident at Point Reyes and Oakland; that is, data assimilation improves the forecasts. In particular, using a combination of observations and climatology produces a more skillful forecast than using either data source independently. This trend is not as apparent at Vandenburg where the distortion of the flow around nearby Point Conception is expected to affect MBL structure.

To evaluate an overall rank for the experiments, we averaged the summed ordinal ranks over all three stations (see Table 4). Results are presented for the initial conditions only (t = 0 h; column 1), forecasts only (t = 6, 12, 18, 24 h; column 2), and all times (column 3). Note that climatological information, when used independent of the coastal data, verifies very poorly at the initial time, but fares very well through the forecast times. This is because the MBL height climatology does not necessarily reflect local conditions at the coast, but does dramatically improve the MBL structure offshore. Since the source region for the coastal PBL is offshore, benefits from proper initialization of the MBL are realized through the forecast period only as air reaches the coastal zone from well offshore. When averaged

TABLE 2. Comparison of observed and model-simulated structure in the California coastal zone. All model values represent average model error (model observed) over five verification times (0000, 0600, 1200, 1800 UTC 4 Aug 1990, and 0000 UTC 5 Aug 1990) except "observations," which are average observed values determined from rawinsondes at the verification times. PBL is the boundary layer depth from the surface to the base of the inversion; DT is the change in temperature through the inversion layer; $-dT/dP$ is the temperature gradient through the inversion layer; DQ is the change in water vapor mixing ratio through the inversion layer; $-dQ/dP$ is the mixing ratio gradient through the inversion layer; TSFC is the surface temperature; WDIR and WSPD are surface wind direction and speed, respectively; TDDAVE is the average dewpoint depression in the PBL; and QAVE is the average mixing ratio in the 800–900-hPa layer.

Station expt	PBL hPa	DT (°C)	$-dT/dP$ (°C hPa^{-1})	DQ (g kg^{-1})	$-dQ/dP$ [g kg^{-1} hPa^{-1}]	Tsfc (°C)	WDIR (°)	WSPD (m s^{-1})	TDDAVE (°C)	QAVE (g kg^{-1})
Point Reyes										
Observations	52.0	14.1	0.30	−4.8	−0.22	14.0	263	3.5	1.0	4.8
CNTL	−48.2	−5.6	−0.22	+1.0	+0.18	+0.5	+28	+2.3	+1.0	−0.7
BSLN	−44.4	−2.2	−0.13	−0.2	+0.13	−0.7	+23	+1.8	−0.6	−1.3
OBSMW	−32.8	−2.8	−0.13	+0.1	+0.15	−0.7	−15	−0.4	−0.6	−0.8
OBSM	−37.4	−2.4	−0.15	+0.5	+0.16	−1.0	−12	+0.9	−0.7	−0.7
MBLI	−22.6	−0.4	−0.07	−0.6	+0.11	−1.2	+38	+2.8	−0.9	−2.4
OBSMBL	−14.0	−1.4	−0.11	+0.2	+0.11	−1.1	+30	+2.4	−0.8	−1.1
Oakland										
Observations	50.8	12.3	0.26	−6.6	−0.91	13.4	283	3.8	2.8	3.6
CNTL	−35.8	−3.4	−0.17	+2.2	+0.86	−0.4	−37	−0.9	+0.5	+0.6
BSLN	−34.4	−1.7	−0.09	+2.3	+0.82	−1.3	−47	−0.9	+0.1	−1.0
OBSMW	−29.8	−1.3	−0.09	+1.8	+0.83	−2.0	−50	−1.4	−1.2	0.0
OBSM	−27.0	−1.6	−0.11	+2.1	+0.84	−0.6	−55	−0.6	−0.7	+0.5
MBLI	−21.6	+0.4	−0.04	+1.1	+0.81	−2.2	−38	−0.7	−1.3	−1.1
OBSMBL	−16.2	+0.4	−0.07	+1.9	+0.83	−1.9	−40	−1.0	−1.3	−0.2
Vandenburg										
Observations	47.4	12.9	0.44	−8.4	−0.67	15.0	249	2.5	2.9	3.3
CNTL	−45.6	−6.6	−0.35	+2.6	+0.56	+1.8	−2	+2.2	−0.2	+0.5
BSLN	−30.8	−4.0	−0.33	+3.7	+0.57	+0.8	−6	+2.9	−2.0	+2.2
OBSMW	−21.2	−4.1	−0.31	+4.5	+0.59	+0.4	−7	+3.0	−1.9	+1.9
OBSM	−21.0	−3.9	−0.30	+4.4	+0.58	+0.7	−3	+3.2	−1.8	+1.5
MBLI	−18.4	−3.1	−0.31	+5.7	+0.61	−0.1	−1	+4.2	−2.4	+3.2
OBSMBL	−12.8	−3.3	−0.30	+5.3	+0.60	−0.7	−7	+3.4	−2.1	+1.7

TABLE 3. Average ordinal ranks based on model error. Lower numbers denote greater skill.

Station Expt	PBL	DT	$-dT/dP$	DQ	$-dQ/dP$	Tsfc	WDIR	WSPD	TDDAVE	QAVE	Sum of ranks
Point Reyes											
CNTL	5.3	6.0	6.0	3.8	5.3	3.4	3.1	4.0	3.8	3.1	43.8
BSLN	4.8	3.1	3.1	4.4	3.0	3.0	4.4	3.4	3.4	4.8	37.1
OBSMW	3.4	3.6	3.6	2.1	3.9	3.0	5.0	3.1	3.1	2.5	31.4
OBSM	4.2	4.2	4.2	3.8	4.3	3.3	3.6	3.4	3.4	2.5	37.2
MBLI	2.2	1.5	1.5	3.8	2.2	4.2	3.4	4.2	4.2	5.4	32.7
OBSMBL	1.1	2.6	2.6	3.1	2.3	4.1	3.5	3.1	3.1	2.7	27.8
Oakland											
CNTL	5.2	5.4	5.6	3.9	5.1	2.6	3.6	3.4	2.7	3.8	41.3
BSLN	4.8	3.3	2.3	2.4	3.0	4.8	3.4	2.4	4.8	2.5	33.7
OBSMW	4.0	3.2	3.6	3.3	3.5	3.1	4.2	4.2	4.7	3.9	37.7
OBSM	3.1	4.0	4.5	3.6	4.7	2.4	2.9	2.9	3.6	4.6	37.6
MBLI	2.1	3.2	2.2	3.2	1.8	4.5	4.3	4.3	2.7	3.6	30.4
OBSMBL	1.8	1.9	2.8	4.6	2.9	3.6	3.8	3.8	2.5	2.6	29.3
Vandenburg											
CNTL	5.9	6.0	5.2	1.9	2.8	5.9	4.0	1.8	2.6	1.0	37.1
BSLN	4.5	2.7	3.6	2.5	3.0	2.9	4.0	2.2	4.1	3.4	32.9
OBSMW	3.2	4.0	3.2	3.2	3.6	3.5	2.0	3.1	3.3	4.7	33.8
OBSM	3.0	3.6	2.9	3.2	2.7	3.3	3.6	4.3	3.1	3.3	33.0
MBLI	2.8	2.2	2.7	5.2	4.1	2.6	4.8	5.3	3.8	4.8	38.3
OBSMBL	1.6	2.5	3.4	5.0	4.8	2.8	2.6	4.3	4.1	3.8	34.9

TABLE 4. Average of summed ordinal ranks over all stations.

Expt	Average of summed ordinal ranks for initial conditions	forecasts only	all times
CNTL	39.5	41.0	40.7
BSLN	39.8	33.3	34.6
OBSMW	30.2	35.3	34.3
OBSM	29.7	37.5	35.9
MBLI	42.7	31.6	33.8
OBSMBL	28.2	31.3	30.7

over all times, OBSMBL is clearly the best initialization strategy in this case.

Finally, Fig. 18 shows the temporal evolution of forecast skill: squares (NOFDDA) show the average performance of experiments that use no data assimilation (CNTL and BSLN), circles (OBS) show the average performance of experiments that use only obs nudging (OBSMW and OBSM), and triangles show skill of the single experiment where both observations and climatological information are used (OBSMBL). The open symbols to the right are the average values over all five verification times. At $t = 0$ h, the FDDA experiments show a distinct improvement over NOFDDA experiments. Note, however, that after 6–12 h, the obs-nudging experiments lose most of their earlier advantage over the NOFDDA experiments. This is a consequence of the advection of poorly developed upstream MBL conditions (see section 6a). With the addition of the climatological information in OBSMBL, however, superior skill is maintained after 6 h.

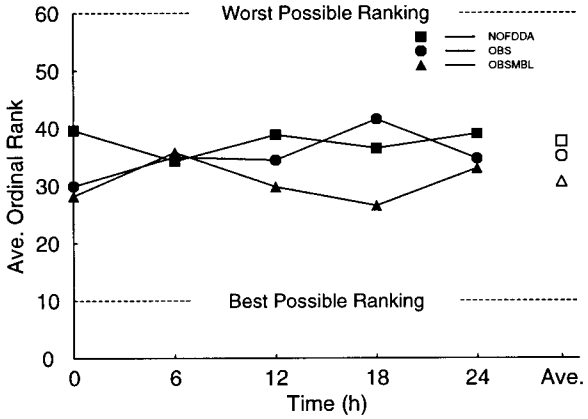

FIG. 18. Temporal evolution of ordinal rankings by FDDA data type.

7. Summary

Initialization of limited area models over the data-sparse ocean remains a difficult problem. Despite advances in satellite remote sensing and automated observing systems, the day-to-day vertical structure of the marine boundary layer is largely unknown over vast regions of the world's oceans. The hypothesis that climatological MBL information and conventional data may be used together to improve initial conditions and short-range mesoscale numerical forecasts in the coastal zone has been investigated along the U.S. west coast during summertime using the the PSU–NCAR MM5.

For this purpose, a new marine boundary layer initialization scheme was developed to demonstrate that climatological information over the northeast Pacific Ocean can be used to advantage in the offshore, data-void regions. The MBLI used Neiburger's (1960) MBL-depth climatology to compute target profiles of temperature and water vapor mixing ratio toward which the model was continuously nudged during a 12-h preforecast initialization period.

Six experiments were performed to test the effectiveness of different initialization strategies: two control experiments (i.e., no FDDA) and four FDDA experiments. Two of the FDDA experiments used a standard MM5 FDDA option (obs nudging). The third and fourth FDDA experiments used the new MBLI scheme alone or in combination with obs nudging. The objective of this investigation was to determine whether the addition of the climatological information showed sufficient impact on skill in these preliminary experiments to warrant a more thorough evaluation over many cases and perhaps with alternate assimilation methodologies.

The results of the experiments were as follows.

- The MBLI scheme established realistic horizontal and vertical structure of the MBL in the coastal zone.
- The average forecast error in the MBL depth for the 24-h period at the coast was significantly reduced (65%) when summertime climatological information was used to initialize the upstream, data-sparse region offshore.
- The use of climatological information to initialize the MBL reduced the time required for the model to produce a realistic MBL by a factor of 2–3.
- Assimilation of only the coastal observations clearly improved the initial conditions and coastal forecasts for the first 6–12 h. After 12 h, the poor quality of conditions offshore (supplied mostly from the NCEP global model) propagated into coastal areas, so that forecasts were not significantly improved compared to the no-FDDA ''control'' experiments.
- Parameterization of atmospheric radiation in stratus clouds was important for simulating the large vertical gradients in temperature and moisture commonly observed at the top of the MBL.
- Vertical resolution of ~15 hPa (100–150 m) through the boundary layer was not sufficient to simulate the observed vertical gradients at the top of the MBL.
- The height of MBL clouds was quite sensitive to the initialization method. Without the use of climatological information in the MBL, the MBL clouds had very low ceilings (<60 m) or were surface based at the end of a 24-h forecast. Cloud ceilings in experi-

ments using MBLI exhibited MBL cloud ceilings averaging 350–450 m.
- Forecasts of the horizontal distribution of MBL clouds were moderately skillful after 12 h and less dependent on the initialization technique.
- The combination of conventional data in the coastal zone and climatology offshore produced better initial conditions and forecasts than did either data source used independently.

In summary, the use of climatological information in the MBLI scheme improved the simulated MBL structure significantly in this case compared to all experiments that were initialized from global model analyses alone or when coastal soundings were added. The general structure established by the MBLI was maintained as it evolved within the forecast model throughout the 24-h period. Positive impacts were noted on forecasts in the coastal zone and offshore.

This study has demonstrated the proof of concept that additional information available in marine–atmospheric climatologies or from appropriate conceptual models may be used to improve the simulated MBL structure, in data-sparse regions of the world's oceans. The results of the preliminary investigation shown here, although based on one very representative summertime case, cannot prove that such an approach necessarily will be successful in routine applications. However, they imply strongly that a more thorough evaluation of assimilation techniques, which include climatological information, over many cases, is warranted. Further benefits could be achieved by improvements in the model physical parameterizations important for MBL structure. For example, a more advanced boundary layer scheme and better stratus cloud radiation physics could improve the simulation of the MBL and the marine inversion. Higher vertical resolution also would contribute to more accurate simulation of the detail in the MBL structure (e.g., Stauffer and Seaman 1999).

Acknowledgments. This research was supported by the U.S. Navy under Contract N00039-92-C-0100, Tasks 07A-1002 and 07A-2015. The authors are grateful to Dale Leipper for his thoughtful comments and suggestions.

REFERENCES

Ballard, S. P., B. W. Golding, and R. N. Smith, 1991: Mesoscale model experimental forecasts of the Haar of northeast Scotland. *Mon. Wea. Rev.,* **119,** 2107–2123.

Beardsley, R. C., C. E. Dorman, C. A. Friehe, L. K. Rosenfeld, and C. D. Winant, 1987: Local atmospheric forcing during the Coastal Dynamics Experiment. I: A description of the marine boundary layer and atmospheric conditions over a northern California upwelling region. *J. Geophys. Res.,* **92,** 1467–1488.

Benjamin, S. G., and N. L. Seaman, 1985: A simple scheme for objective analysis in curved flow. *Mon. Wea. Rev.,* **113,** 1184–1198.

Bond, N. A., C. F. Mass, and J. E. Overland, 1996: Coastally trapped wind reversals along the United States west coast during the warm season. Part I: Climatology and temporal evolution. *Mon. Wea. Rev.,* **124,** 430–445.

Bretherton, C. S., P. Austin, and S. T. Siems, 1995: Cloudiness and marine boundary layer dynamics in the ASTEX Lagrangian experiments. Part II: Cloudiness, drizzle, surface fluxes, and entrainment. *J. Atmos. Sci.,* **52,** 2724–2735.

Bridger, A. F. C., W. C. Brick, and P. F. Lester, 1993: The structure of the marine inversion layer off the central California coast: Mesoscale conditions. *Mon. Wea. Rev.,* **121,** 335–351.

Brost, R. A., D. H. Lenschow, and J. C. Wyngaard, 1982: Marine stratocumulus layers. Part I: Mean conditions. *J. Atmos. Sci.,* **39,** 800–817.

Burk, S. D., and W. T. Thompson, 1996: The summertime low-level jet and marine boundary layer structure along the California coast. *Mon. Wea. Rev.,* **124,** 668–686.

Byers, H. R., 1930: Summer sea fogs of the central California coast. *Univ. Calif. Publ. Geogr.,* **3,** 291–338.

Chao, S.-Y., 1985: Coastal jets in the lower atmosphere. *J. Phys. Oceanogr.,* **15,** 361–371.

Dorman, C. E., 1985: Evidence of Kelvin waves in California's marine layer and related eddy generation. *Mon. Wea. Rev.,* **113,** 827–839.

Dudhia, J., 1989: Numerical study of convection observed during the Winter Monsoon Experiment using a mesoscale two-dimensional model. *J. Atmos. Sci.,* **45,** 3077–3107.

——, 1993: A nonhydrostatic version of the Penn State/NCAR mesoscale model: Validation tests and simulation of an Atlantic cyclone and cold front. *Mon. Wea. Rev.,* **121,** 1493–1513.

Duynkerke, P. G., and A. G. M. Driedonks, 1987: A model for the turbulent structure of the stratocumulus-topped atmospheric boundary layer. *J. Atmos. Sci.,* **44,** 43–64.

——, and P. Hignett, 1993: Simulation of diurnal variation in a stratocumulus-capped marine boundary layer during FIRE. *Mon. Wea. Rev.,* **121,** 3291–3300.

——, H. Zhang, and P. J. Jonker, 1995: Microphysical and turbulent structure of nocturnal stratocumulus as observed during ASTEX. *J. Atmos. Sci.,* **52,** 2763–2777.

Edinger, J. G., 1963: Modification of the marine layer over coastal southern California. *J. Appl. Meteor.,* **2,** 706–712.

Elliott, D. L., and J. J. O'Brien, 1977: Observational studies of the marine boundary layer over an upwelling region. *Mon. Wea. Rev.,* **105,** 86–98.

Gerber, H., S. Chang, and T. Holt, 1989: Evolution of a marine boundary-layer jet. *J. Atmos. Sci.,* **46,** 1312–1326.

Grell, G. A., J. Dudhia, and D. R. Stauffer, 1994: A description of the fifth-generation Penn State/NCAR Mesoscale Model (MM5). NCAR Tech. Note 398 + STR, 122 pp.

Hu, Y. X., and K. Stamnes, 1993: An accurate parameterization of the radiative properties of water clouds suitable for use in climate models. *J. Climate,* **6,** 728–742.

Lacis, A. A., and J. E. Hansen, 1974: A parameterization of the absorption of solar radiation in the earth's atmosphere. *J. Atmos. Sci.,* **31,** 118–133.

Mass, C. F., and M. D. Albright, 1987: Coastal southerlies and alongshore surges of the west coast of North America: Evidence of mesoscale topographically trapped response to synoptic forcing. *Mon. Wea. Rev.,* **115,** 1707–1738.

——, and N. A. Bond, 1996: Coastally trapped wind reversals along the United States west coast during the warm season. Part II: Synoptic evolution. *Mon. Wea. Rev.,* **124,** 446–461.

Neiburger, M., 1960: The relation of air mass structure to the field of motion over the eastern North Pacific Ocean in summer. *Tellus,* **12,** 31–40.

Nicholls, S., and J. Leighton, 1986: An observational study of the structure of stratiform cloud sheets. Part I: Structure. *Quart. J. Roy. Meteor. Soc.,* **112,** 431–460.

Oliver, D. A., W. S. Lewellen, and G. G. Williamson, 1978: The interaction between turbulent and radiative transport in the de-

velopment of fog and low-level stratus. *J. Atmos. Sci.,* **35,** 301–316.

Rotunno, R., and Coauthors, 1992: *Coastal Meteorology: A Review of the State of the Science.* National Academy Press, 99 pp.

Simon, R. L., 1977: The summertime stratus over the offshore waters of California. *Mon. Wea. Rev.,* **105,** 1310–1314.

Slingo, A., 1989: GCM parameterization for the short-wave radiative properties of water clouds. *J. Atmos. Sci.,* **46,** 1419–1427.

——, R. C. Wilderspin, and R. N. B. Smith, 1989: Effect of improved physical parameterizations on simulations of cloudiness and the Earth's radiation budget. *J. Geophys. Res.,* **94D,** 2281–2301.

Stauffer, D. R., and N. L. Seaman, 1990: Use of four-dimensional data assimilation in a limited-area mesoscale model. Part I: Experiments with synoptic-scale data. *Mon. Wea. Rev.,* **118,** 1250–1277.

——, and ——, 1994: Multiscale four-dimensional data assimilation. *J. Appl. Meteor.,* **33,** 416–434.

——, and ——, 1999: Intercomparison of turbulence parameterizations for simulating coastal-zone marine boundary layer structure. Preprints, *Third Conf. on Coastal Atmospheric and Oceanic Prediction Processes,* New Orleans, LA, Amer. Meteor. Soc., 7–12.

——, ——, and F. S. Binkowski, 1991: Use of four-dimensional data assimilation in a limited-area mesoscale model. Part II: Effects of data assimilation within the planetary boundary layer. *Mon. Wea. Rev.,* **119,** 734–754.

Stephens, G. L., 1978: Radiation profiles in extended water clouds. I: Theory. *J. Atmos. Sci.,* **35,** 2111–2122.

Thompson, W. T., S. D. Burk, and J. Rosenthal, 1997a: An investigation of the Catalina eddy. *Mon. Wea. Rev.,* **125,** 1135–1146.

Thompson, W. T., T. Haack, J. D. Doyle, and S. D. Burk, 1997b: A nonhydrostatic mesoscale simulation of the 10–11 June 1994 coastally trapped wind reversal. *Mon. Wea. Rev.,* **125,** 3211–3230.

Winant, C. D., C. E. Dorman, C. A. Friehe, and R. C. Beardsley, 1988: The marine layer off northern California: An example of supercritical channel flow. *J. Atmos. Sci.,* **45,** 3588–3605.

Zemba, J., and C. A. Friehe, 1987: The marine atmospheric boundary layer jet in the Coastal Ocean Dynamics Experiment. *J. Geophys. Res.,* **92C,** 1489–1496.

Zhang, D. L., and R. A. Anthes, 1982: A high-resolution model of the planetary boundary layer—Sensitivity tests and comparisons with SESAME-79 data. *J. Appl. Meteor.,* **21,** 1594–1609.